NASA Technical Memorandum 79303

(NASA-TM-79303) COMBUSTION OF SOLID CARBON RODS IN ZERO AND NORMAL GRAVITY (NASA) 32 p HC A03/MF A01 CSCL 21B

N80-13404

Unclas
G3/34 46312

COMBUSTION OF SOLID CARBON RODS IN ZERO AND NORMAL GRAVITY

C. M. Spuckler, F. J. Kohl,
R. A. Miller, C. A. Stearns
Lewis Research Center
Cleveland, Ohio

and

K. J. DeWitt
The University of Toledo
Toledo, Ohio

Prepared for the
Seventy-second Annual AIChE Meeting
San Francisco, California, November 25-29, 1979

COMBUSTION OF SOLID CARBON RODS IN ZERO AND NORMAL GRAVITY

by C. M. Spuckler, F. J. Kohl, R. A. Miller, C. A. Stearns
National Aeronautics and Space Administration
Lewis Research Center
Cleveland, Ohio 44135

and

K. J. De Witt
The University of Toledo
Toledo, Ohio 43606

ABSTRACT

In order to investigate the mechanism of carbon combustion, normal and zero gravity experiments were conducted in which spectroscopic carbon rods were resistance ignited and burned in an oxygen environment. Direct mass spectrometric sampling was used in the normal gravity tests to measure gas phase concentrations. The gas sampling probe was positioned near the circumference of the horizontally mounted carbon rods, either at the top or at angles of 45° or 90° from the top, and yielded concentration profiles of CO_2, CO, and O_2 as a function of distance from the carbon surface. The experimental concentrations were compared to those predicted by a stagnant film model. Zero gravity droptower tests were conducted in order to assess the effect of convection on the normal gravity combustion process. The ratio of flame diameter to rod diameter as a function of time for oxygen pressures of 5, 10, 15, and 20 psia was obtained for three different diameter rods. It was found that this ratio was inversely proportional to both the oxygen pressure and the rod diameter.

E-255

INTRODUCTION

In recent years, a new emphasis has been placed on research involving the production of energy from new or existing sources. One of the areas of interest is solid combustion oriented toward an understanding of the true mechanism involved in the combustion of coal. The chemical and physical processes involved in the combustion of a solid depend in part on the nature of the solid. Many solids burn in a manner similar to liquid fuels, that is, the surface of the fuel sublimates, the vapor then mixing with oxygen and burning to produce a flame zone.

Combustion of carbonaceous solids, such as coal, is complex because it takes place in two stages. The coal first pyrolyzes on being heated, with the volatile gases being driven from the solid through pores and cracks to the outside environment where they mix with oxygen and burn. After all volatiles have been driven off, mainly solid carbon remains, which then burns via reactions on the surface and in the pores. During this latter process, various chemical reactions can occur. The carbon

surface reacts with oxygen to form either carbon monoxide, carbon dioxide, or a combination of both. If carbon monoxide is formed at the surface, a gas phase reaction of the carbon monoxide with oxygen to form carbon dioxide is possible.

To gain a better understanding of the mechanism of coal combustion, it was decided that the process by which carbon ignites and burns should be examined. If the carbon combustion process can be understood, the results should aid in the analysis of the larger problem of coal combustion. The present investigation (1) was undertaken to investigate the mechansim of carbon combustion. Both normal and zero gravity experiments were conducted to assess the effect of convection on the normal gravity combustion process.

PROPOSED CARBON COMBUSTION MODELS

Carbon is one of the solids that burns with a surface reaction, and various models for the combustion of carbon have been proposed (2-7). The products of combustion and the mechanism of the combustion process depend on the carbon surface temperature. In the low temperature model, surface temperature below approximately 770 K, carbon is burned to carbon dioxide at the surface by the reaction $C^{(s)} + O_2^{(g)} \rightarrow CO_2^{(g)}$. This model along with the assumed concentration and temperature profiles is presented in figure 1.

At moderate temperatures, between 770 and 1370 K, both carbon dioxide and carbon monoxide are formed at the surface by the two surface reactions, $C^{(s)} + O_2^{(g)} \rightarrow CO_2^{(g)}$, and $2C^{(s)} + O_2^{(g)} \rightarrow 2CO^{(g)}$. There is no subsequent oxidation of carbon monoxide in the gas phase. This model is presented in figure 2.

For high surface temperatures, above 1370 K, four models have been proposed. Ubhayakar and Wiliams (2) proposed a model in which carbon reacts with oxygen at the surface to form carbon monoxide through the reaction $2C^{(s)} + O_2^{(g)} \rightarrow 2CO^{(g)}$, with no further reactions occurring in the gas phase. This model is presented in figure 3(a). Fendell (3) proposed a complex high temperature model in which two surface reactions take place. Carbon is oxidized to carbon monoxide through the reaction $2C^{(s)} + O_2^{(g)} \rightarrow 2CO^{(g)}$, and ambient carbon dioxide is reduced to carbon monoxide through the reaction $CO_2^{(g)} + C^{(s)} \rightarrow 2CO^{(g)}$. There is no gas phase oxidation of carbon monoxide. This model is presented in figure 3(b). A third high temperature model has been proposed by Wicke and Wurzbacher (4) and Caram and Amundson (5). In this model, carbon monoxide is formed at the surface through two surface reactions, $C^{(s)} + CO_2^{(g)} \rightarrow 2CO^{(g)}$ and $2C^{(s)} + O_2^{(g)} \rightarrow 2CO^{(g)}$. The carbon monoxide is then burned to carbon dioxide through the homogeneous gas phase reaction $2CO^{(g)} + O_2^{(g)} \rightarrow 2CO_2^{(g)}$. This model is presented in figure 3(c). A fourth, high temperature model, has been proposed by

Spalding (6) and van der Held (7). In this model carbon dioxide is reduced to carbon monoxide at the surface through the reaction $CO_2^{(g)} + C^{(s)} \rightarrow 2CO^{(g)}$. The carbon monoxide diffuses outward, meeting oxygen, and is burned to carbon dioxide through the gas phase reaction $2CO^{(g)} + O_2^{(g)} \rightarrow 2CO_2^{(g)}$. Analytically, the gas phase reaction can be considered to occur with an infinitely fast reaction rate so that a very thin flame sheet forms, or with a finite rate so that a flame zone appears. This model is shown in figure 3(d).

ZERO-GRAVITY APPARATUS, PROCEDURE, AND TEST MATERIALS

Test Facility

The experimental data for this part of the study were obtained in the Zero-Gravity Facility at the Lewis Research Center. A schematic diagram of the facility is shown in figure 4. The facility consists of a concrete-lined 8.5 meter diameter shaft that extends 155 meters below ground level. A steel vacuum chamber, 6.1 meters in diameter and 143 meters high, is contained within the concrete shaft. The pressure in this vacuum chamber is reduced to 13.3 newtons per square meter by utilizing the Center's wind tunnel exhaust system and an exhauster system located in the facility. Tests are conducted from the control room which contains the exhauster control system, the experiment vehicle predrop checkout and control system, and the data retrieval system.

In the Zero-Gravity Facility, the experiment vehicle is allowed to fall freely from the top of the vacuum chamber, resulting in nominally 5 seconds of free-fall time. The words "fall free" mean that there are no guide wires, electrical lines, etc., connected to the vehicle. Therefore, the only force (aside from gravity) acting on the experiment is due to residual air drag. This results in an experiment gravitational environment acting on the vehicle which is estimated to be on the order of 10^{-5} g's maximum.

After the experiment has traversed the total length of the vacuum chamber, it is decelerated in a 3.6 meter diameter, 6.1 meter deep container which is located on the vertical axis of the chamber and filled with small pellets of expanded polystyrene. The deceleration rate (averaging 32 g's) is controlled by the flow of pellets through an area between the experiment vehicle and the wall of the deceleration container.

The experimental vehicle used to obtain the data is shown in figure 5. The overall height was 3 meters and the largest diameter was 1.06 meters. The vehicle consisted of a telemetry section contained in the aft fairing and an experimental section housed in the cylindrical midsection.

The details of the experiment section are shown in figure 6. The spherical tanks at the top section are part of a N_2 fire extinguishment system which was used as a safety precaution at the completion of each test. The bulk of the experimental equipment was contained in the central portion of the drop module and consisted of a combustion chamber with a carbon rod holder, two high speed cameras, power supplies, electrical control box, and plumbing used to fill and evacuate the chamber.

A cross-sectional schematic of the combustion chamber is shown in figure 7. The combustion chamber was a 78.74 cm long by 39.62 cm diameter cylinder with a 19.81 cm radius spherical cap. This resulted in an internal volume of approximately 1.1×10^5 cm^3. The walls of the chamber were 0.476 cm thick stainless steel. There were four ports for electrical and instrumentation wires. There were also two viewing ports that were used to photograph the combustion process. One viewing port was 12.70 cm from the bottom of the chamber and the other one was at the top of the spherical cap. The chamber was split 25.40 cm from the bottom so that the top part of the chamber could be removed for replacement of the experiment.

The carbon rod burning apparatus was inside the combustion chamber as shown in figure 8. This apparatus, shown in figure 9, consisted of a 22.86 cm square by 0.476 cm thick stainless steel plate with two 0.476 cm diameter bolts 3.81 cm long in it. The two bolts were 7.62 cm apart. Lead wires were held to the bolts by tie-downs, at the ends of which were junctions that connected to tungsten electrodes. These electrodes were pushed into the ends of the carbon rods. The diameter of the electrodes varied depending upon the diameter of the carbon rod used in the test. When a 0.614 cm diameter or 0.457 cm diameter carbon rod was used, the electrodes were 0.025 cm in diameter. When a 0.305 cm diameter carbon rod was used, the electrodes were 0.102 cm in diameter.

Two cameras were used to photograph the combustion process. One camera was located at the side viewing port and photographed the end of the carbon rod. This camera ran at 400 frames/sec. The other camera was positioned at the top of the combustion chamber and photographed the length of the rod from the top. This camera ran at 200 frames/sec. A timing mark every 0.01 second was put on the edge of the film. Also, a continuous mark was put on the edge of the film before the vehicle was released. At release, the mark was cut off, giving a reference time for the start of zero-gravity. Power to ignite the carbon rod was supplied by rechargeable lead acid battery packs. For tests using the 0.615 cm diameter rod, 48 volts were used and the current drawn was approximately 220 amps. For the 0.457 and the 0.305 cm rods, the corresponding volts and amps were 32 and 16 and 140 and 50, respectively. A separate power supply using rechargeable nickel-cadmium batteries was used to supply power to the other equipment in the drop vehicle.

Test Materials

Ultra-Carbon spectroscopic carbon rods 0.615, 0.457, and 0.305 cm in diameter were used. The rods were cut into two inch lengths, and electrode holes were drilled 0.397 cm deep into the ends of the rods. The atmosphere for the tests was oxygen with a 0.5 ppm water vapor content.

Test Procedure

Prior to each run, the combustion chamber was wiped clean. Before the carbon rod was inserted into the holder, the holes in the ends of the rod

were filled with silver brazing powder. The powder was used to reduce the contact resistance between the rod and the electrodes. The combustion chamber was then closed and sealed. The chamber was evacuated and purged with dry nitrogen three times before it was filled with oxygen.

The proper voltage for ignition of the size rod used in the test was set, along with the amount of time power would be allowed to flow through the carbon rods. Power to ignite the carbon rods was set to go on 0.045 second after the vehicle was released. This prevented free convection currents, arising from the heated rod, from being set up inside the combustion chamber.

The vehicle was positioned at the top of the vacuum chamber as shown in figure 10. It was suspended by the support shaft on a hinged-plate release mechanism. During vacuum chamber pumpdown and prior to release, monitoring of experimental vehicle systems was accomplished through an umbilical cord attached to the top of the support shaft. Electrical power was supplied from ground equipment. The system was switched to internal power a few minutes before release. The vehicle was released by pneumatically shearing a bolt that was holding the hinged plate in the closed position. No measureable disturbances were imparted to the experiment vehicle by this release procedure.

The total free fall test time obtained was 5.16 seconds. During the test drop, the vehicle's trajectory and deceleration were monitored on closed circuit television. Following the drop, the vacuum chamber was vented to the atmosphere and the experiment was returned to ground level.

The burning rods were photographed on high speed film which was examined on a motion picture analyzer. From the film showing the end view of the rod, flame diameters were measured as a function of time.

RESULTS AND DISCUSSION

Tests burning 0.615, 0.475, and 0.305 cm diameter by 5.08 cm long carbon rods in 5, 10, 15, and 20 psia oxygen environments were conducted under zero gravity conditions. The rods were ignited in zero gravity by passing an electric current through them for a set time, which was usually less than 1 second. The rods were then allowed to burn, supported only by their own combustion, for a period of approximately 4 seconds in zero gravity. In some tests, the power to the carbon rod was not left on long enough to completely ignite the rod. In all except one of these incomplete ignition tests, the rod glowed initially and then decreased in intensity through the duration of the test, indicating that the reaction was being quenched. In one case involving a 0.615 cm diameter rod in 20 psia oxygen, the flame flickered and went out as the rod cooled during the test. In all other tests where sustained burning occurred in zero gravity, a blue flame surrounded the rod. Photographs of the end of the burning rods for two tests are shown in figures 11 and 12. In figure 11, a 0.615 cm diameter rod in 20 psia oxygen is shown, and the same diameter rod in 5 psia oxygen is shown in figure 12. From these photographs it can be seen that a symmetrical blue flame extending from the surface surrounds the rod, indicating that the CO formed at the surface is being burned to CO_2 in a gas phase reaction through out the region.

A representative sample of the data obtained in the zero gravity tests is presented in figures 13 and 14. The ratio of flame diameter to rod diameter is plotted as a function of time. Figure 13 shows the effect of pressure on flame diameter for a 0.615 cm diameter rod, and illustrates that as the pressure decreases, the ratio of flame diameter to rod diameter increases. Figure 14 shows the effect of rod diameter on the ratio of flame diameter to rod diameter for 20 psia pressure. The ratio of flame diameter to rod diameter is seen to decrease as the rod diameter increases. Both figures show that the ratio of flame diameter to rod diameter tends to increase less rapidly as the burning time increases. At larger times above 4 seconds, especially for large diameter rods and high pressure, the data seems to indicate that the ratio of flame diameter to rod diameter may be approaching a steady state value.

The data obtained for each zero gravity test were curve fitted numerically using an exponential fit. The equations obtained are available in reference 1, and show that the variation within a test was less than the variation between tests that were conducted with the same diameter rod and at the same pressure. The reason for the difference between tests is that there was no way to control the surface temperature of the rod. Also, there was not enough time for the carbon rod to reach an equilibrium burning temperature in the approximately 5 seconds of drop time.

CONCLUSIONS FOR ZERO GRAVITY TESTS

The blue flame surrounding the carbon rod under zero-gravity shows a gas phase reaction occurred, in which carbon monoxide was oxidized to carbon dioxide. This means the carbon rod is burning according to one of the high temperature models that allows a gas phase reaction. Because the flame extends from the surface of the rod, the carbon would seem to be burning according to the model presented by Wicke and Wurzbacker (4) or Caram and Amundson (5). If the flame did not extend from the surface, that is, if it stood off from the surface, the carbon would be burning according to the model presented by Spalding (6). To confirm which high temperature model is correct would require concentration profiles. If the O_2 concentration extends to the surface of the rod, the model presented by Wicke and Wurzbacker (4) or Caram and Amundson (5) would be correct. If the O_2 concentration goes to zero before the surface of the rod is reached, the model presented by Spalding (6) would be correct. The normal gravity models indicate that the surface temperature should be above 1370 K when a surface reaction occurs. But, because these tests were conducted under zero-gravity conditions, the surface temperature may be different than that indicated by the model. To obtain the surface temperature an optical technique would have to have been used, but this was not possible in the zero-gravity facility. From the zero-gravity data it was found that the ratio of flame diameter to rod diameter increases as the pressure decreases, and decreases as the rod diameter increases. Because of the various parameters involved in the carbon combustion process, surface temperatures and concentration and temperature profiles are needed to accurately model the zero-gravity combustion process. The data obtained from this experiment can be used to properly design an in-space experiment, such as for Spacelab, where the information required to model the combustion process can be obtained.

NORMAL GRAVITY APPARATUS AND PROCEDURE

Test Facility

The experimental system used to study the products of combustion from a burning carbon rod consisted of a carbon rod igniter and a modulated molecular beam mass spectrometric sampler.

The carbon rod igniter and holder are shown in figure 15. In all of the normal gravity tests, 0.615 cm diameter by 5.08 cm long carbon rods were used. The carbon rod was held by two tungsten electrodes, which were 0.159 cm in diameter and extended through two copper poles. The center of the carbon rod was 6.1 cm above the flow straightener. A glass cylinder with a 10.80 cm inside diameter and a height of 11.43 cm surrounded the carbon rod holder.

The rods were burned at atmospheric pressure in oxygen with a water vapor content of 6 ppm. A volumetric flow rate of 0.15 l/sec was set by a needle valve and measured with a calibrated rotameter. This volumetric flow rate, which had to be used to make up for the gases drawn off by the sampling probe, corresponded to a 5.63 cm/sec flow rate past the rod. The oxygen entered through the bottom of the lower section of the carbon rod holder, which was a 7.62 cm long cylinder with a 6.86 cm inside diameter. The oxygen flowed through a screen and then through a section containing plastic balls 0.572 cm in diameter in order to spread the flow. Finally, the oxygen passed through a Hastelloy X honeycomb flow straightener. The burner was supported by mechanical devices which facilitated micrometer movement in three mutually perpendicular directions. Power to ignite the carbon rod was supplied by a 48 volt power supply.

Direct mass spectrometric analysis of the species in the atmospheric pressure flame zone surrounding the carbon rod was accomplished with a modulated molecular beam mass spectrometer sampler, shown in figure 16. This technique sampled the species while preserving their dynamic and chemical integrity. The sampler, described in more detail in reference 8, is shown schematically in figure 17. Atmospheric pressure sampling was accomplished by drawing a sample through either a 0.20 mm diameter Pt-10% Rh orifice shown in figure 17, or through a quartz sampling probe with a 0.20 mm diameter orifice shown in figure 18. Quartz sampling probes with orifice diameters of 0.03, 0.13, and 0.25 mm were also tried. The small probes (0.03 and 0.13 mm) plugged by small flakes from the carbon surface and the 0.25 mm orifice was so large that the sampling system could not be pumped down. The Pt-10% Rh orifice was used to obtain samples at the top of the rod, 0° position, and the quartz probe was used to obtain samples at positions of 45° and 90° from the top of the rod.

To sample the center portion of the flow from the sampling orifice or probe, the stream was passed through a skimmer cone with an orifice diameter of 0.81 mm and an included angle of 60°. The distance between the sampling orifice or the top plate of the quartz sampling probe and the skimmer orifice was 3.17 cm. For this physical configuration with the nominal pumping speeds indicated in figure 17, first and second stage pressures were approximately 1.5×10^{-3} and 8×10^{-6} torr, respectively, when sampling room temperature atmospheric pressure gas. When the gas temperature was increased to 1000° C, these pressures were 7×10^{-4} and 1×10^{-6} torr, respectively. Stage I

pressures were read with a capacitance manometer, and the other three stage pressures were read with ion gauges. The molecular beam from the skimmer was chopped by a motor driven two-toothed chopper wheel located in Stage II. A chopping frequency of 150 Hertz was used and a reference signal at this frequency was derived from a light bulb and a photo diode coupled to the chopper wheel. The chopped molecular beam then passed to the electron bombardment ion source of a quadrupole mass spectrometer. The quadrupole filter with 1.6 cm diameter poles had a mass range extending to over 600 AMU. A Channeltron electron multiplier was employed to multiply the ion current output of the ion source-quadrupole filter. Two channels of current output were measured as a function of quadrupole filter tuning. One channel measured the total chopped ion current, and the other channel measured only the component of the ion current signal in phase with the chopper. The second channel was driven by a lock-in amplifier-phase sensitive detector system tuned to the chopper frequency reference signal. The gaseous species in the flame were measured by recording the in-phase component of the ion current for respective values of mass to charge ratio. The accuracy of the mole fractions obtained is uncertain because the system was not calibrated for such mass dependent factors as quadrupole mass filter transmission, multiplier gain, or Mach number focusing. But because the mass range used was narrow, 26 to 46 AMU, the errors associated with the mass dependent factors are estimated to be less than 10 percent.

Procedure

The sampling orifice to be used in the test was attached to the mass spectrometric sampler. The sampling apparatus was pumped down and the quadrupole mass filter range was set for the range of 26 to 46 AMU with a rate of 0.2 sec/AMU, so spectra were recorded every 4 seconds.

The holes in the ends of the carbon rods were filled with silver brazing powder before they were put into the carbon rod holder in order to reduce the contact resistance between the electrodes and the carbon rod.

For tests where gas samples were taken at the top of the rod, the glass cylinder was moved up to the plate holding the orifice, and the carbon rod was positioned 0.69 cm below the sampling orifice. After the rod was ignited, it was moved toward the sampling orifice. At least two gas samples were taken at each position. The distance the carbon rod was moved was measured with a dial indicator that had increments of 0.003 cm. For the tests where the quartz probe was used to sample the gases, the probe was set 0.025 cm from the surface and left in this position while the rod burned. Because the quartz sampling probe was lower than the Pt-10% Rh probe, the glass cylinder was open at the top. To eliminate ambient air from entering the carbon rod holder, aluminum foil with a slot in it for the sampling probe was placed on top of the glass cylinder.

Before a rod was ignited, the carbon holder assembly was purged with oxygen. The gas species in the carbon holder assembly were monitored with the mass spectrometer. The rod was ignited when oxygen was the only gas present in the assembly. Ignition was attained by passing an electrical current through the rod. Power was supplied by a 48 volt power supply. The power was left on until a flame appeared around the carbon rod.

Data Reduction

The ion intensities were corrected for relative ionization cross sections. Cross sections for atoms were taken from Mann (9) and estimated for molecules as 0.75 times the sum of the atomic values. Three rods were photographed in the burning apparatus, and the position of the carbon surface was plotted as a function of time. This data was used to determine the distance the sampling probe was away from the surface.

RESULTS AND DISCUSSION

Concentration profiles of the combustion products of a carbon rod as a function of distance from the surface were obtained for initial sampling probe positions of 90°, 45°, and 0°, with 0° being the top of the rod. The lower part of the rod burned faster than the top of the rod, so that the angle of the probes initially positioned at 45° and 90° changed as the rod burned. In figure 19, the concentrations of O_2, CO_2, and CO as a function of distance from the surface for the 90° quartz sampling probe are presented. The O_2 concentration increases with distance from the surface while the CO_2 and CO concentrations decrease with distance from the surface. The concentration of CO was lower than the concentration of CO_2 except near the surface, that is, less than 0.05 cm from the surface. Also, at this distance the concentration of CO_2 can be seen to level off. None of the concentrations seem to go to zero at the surface, which indicates that the surface reaction at this position was controlled by chemical kinetics and not by diffusion.

The concentration profiles obtained with the quartz probe at the 45° position are presented in figure 20. Again the oxygen concentration increases with distance from the surface, while both the CO_2 and the CO decrease with distance. The oxygen concentration is lower than the CO_2 and CO concentrations very close to the surface. The CO concentration is always lower than the CO_2 concentration. The concentrations if extrapolated to the surface do not appear to equal zero, but the O_2 does indicate that it would have a low value. This again indicates a kinetically controlled reaction at the 45° position.

The concentration profiles obtained with the Pt-10% Rh probe at the top of the rod are presented in figure 21. At this position as at the other positions the O_2 increases with distance from the surface while the CO decreases. The CO_2 at first increases with distance from the surface, reaching a maximum approximately 0.36 cm from the surface, and then starts to decrease. The concentration of CO_2 is higher than that of the other species, except for O_2 at large distances from the surface greater than 0.64 cm. The rate of CO concentration decrease is more rapid near the surface than away from the surface. The concentration of O_2 is lower than the concentration of CO or CO_2 near the surface, approximately 0.20 cm from the surface. Also, at 0.64 cm there is a rapid increase in O_2 and a corresponding rapid decrease in CO_2, indicating that the ambient oxygen in the carbon rod holder assembly is mixing with the combustion products.

The O_2 concentration as a function of distance from the surface for the three sampling positions is presented in figure 22. The O_2 concentration decreases with position from 90° to 0°. The O_2 tends to reach the same

value for the 90° and 45° probe positions at an approximate position of 0.23 cm from the surface. If the concentrations are extrapolated to the surface, it can be seen that the surface concentration decreases considerably from the 90° position to the 45° position. It would be difficult to extrapolate the 0° position to the surface, but if the trend set by the 90° and 45° positions holds, it is very likely that at the 0° position the surface concentration would go to zero. This indicates that the oxygen reaction at the surface is kinetically controlled at both the 90° and 45° positions, but that it is very possible that the reaction at the 0° position is diffusion controlled.

The CO_2 concentration as a function of distance from the surface for the three positions is presented in figure 23. The CO_2 concentration is higher for the 45° probe position than it is for the 90° probe position. The concentrations for these two positions tend to become equal to each other away from the surface, that is at approximately 0.023 cm. The concentrations at the 0° probe position are greater than those at the other two positions. The positive slope of concentrations for the 90° and 0° probe positions indicates that the CO_2 is reacting at the surface to produce CO. The increase of CO_2 with position from 90° to 0° indicates that the combustion products are being convected upward.

The CO concentration as a function of distance from the surface for the three sampling positions is shown in figure 24. The concentrations of CO are approximately the same for the 90° and 45° probe positions except at distances between 0.08 and 0.023 cm from the surface where the CO concentration is lower for the 90° position. The CO concentration at the 0° position is the highest. The data for the 45° and 90° positions are plotted in figures 25(a) and (b). If the data is extrapolated to the surface, it can be seen that the surface concentration for the 45° probe position is greater than that at the 90° position. Therefore the CO concentration at the surface increases with position from 90° to 0°. The increase in CO with decreasing angle can be attributed to convection of the combustion products upward and to CO_2 reacting with carbon, especially at the 0° probe position.

The data from figures 22 to 24 indicate that free convection plays a major role in the combustion process. The decrease of O_2 with decreasing angle indicates that convected O_2 is reacting at the surface and that the O_2 cannot be replenished by molecular diffusion. The increase in CO_2 with decreasing angle also shows this same result, even though it is reacting at the surface to produce CO. The reaction for the O_2 indicates a change in control mechanism from kinetic control at the lower sampling positions to diffusion control at the top of the rod. This change of mechanism may also occur for the CO_2 at the 0° position, but data near the surface, that would be needed to verify this could not be obtained.

Four tests were conducted in which a monochromatic optical pyrometer was used to determine the surface temperature. No gas samples were taken during these tests because the carbon rod holder had to be removed from the mass spectrometer system. The same flow system was used and conditions were kept the same as in the sampling tests. The time average surface temperature of the rod was found to be 1542 K, which is above the minimum surface temperature found in the literature for a gas phase reaction. There was only a few degree temperature difference between the bottom of the rod and the top of the rod.

COMPARISON WITH MATHEMATICAL MODEL

The normal gravity data were compared with a high temperature model in which a homogeneous gas phase reaction took place. The model presented by Caram and Amundson (5) for carbon spheres and flat plates was extended to cylindrical rods. The assumptions inherent in the model are: the atmosphere is dry oxygen, a stagnant film of thickness δ surrounds the rod, end effects are neglected, the rod does not react internally, there are two surface reactions $2C + O_2 \rightarrow 2CO$ and $C + CO_2 \rightarrow 2CO$, there is a gas phase reaction $2CO + O_2 \rightarrow 2CO_2$, physical properties are constant, steady state exists, there is only binary diffusion, flow is only in the radial direction, and the Schwab-Zeldovich approximation $D_{CO} = D_{CO_2} = D_{O_2} = \lambda/\rho C_p$ holds.

The governing equations are

Continuity:

$$\rho r V = \text{const} = q = m_c r_s \left(2R_{O_2} + R_{CO_2}\right) \tag{1}$$

Species:

$$O_2 \qquad \frac{q}{r}\frac{d\omega_{O_2}}{dr} - \frac{\rho D_{O_2}}{r}\frac{d}{dr}\left(r\frac{d\omega_{O_2}}{dr}\right) = -R_{O_2} = -\frac{1}{2}M_{O_2}R_{CO} \tag{2}$$

$$CO_2 \qquad \frac{q}{r}\frac{d\omega_{CO_2}}{dr} - \frac{\rho D_{CO_2}}{r}\frac{d}{dr}\left(r\frac{d\omega_{CO_2}}{dr}\right) = R_{CO_2} = M_{CO_2}R_{CO} \tag{3}$$

$$CO \qquad \frac{q}{r}\frac{d\omega_{CO}}{dr} - \frac{\rho D_{CO}}{r}\frac{d}{dr}\left(r\frac{d\omega_{CO}}{dr}\right) = -R_{CO} = -M_{CO}R_{CO} \tag{4}$$

Energy:

$$\frac{qC_pT_b}{r}\frac{d\tau}{dr} - \frac{\lambda T_b}{r}\frac{d}{dr}\left(r\frac{d\tau}{dr}\right) = \frac{W_{CO}R_{CO}}{2} \tag{5}$$

The surface boundary conditions assume that the flux of a species at the surface is equal to the reaction rate. The surface boundary conditions are:

$$O_2 \qquad -\frac{\rho D_{O_2}}{M_{O_2}}\frac{d\omega_{O_2}}{dr}\bigg|_s + \frac{q\omega_{O_2}}{M_{O_2}r_s} = -R_{O_2} \tag{6}$$

$$CO_2 \qquad -\frac{\rho D_{CO_2}}{M_{CO_2}}\left.\frac{d\omega_{CO_2}}{dr}\right|_s + \frac{q\omega_{CO_2}}{M_{CO_2} r_s} = -R_{CO_2} \tag{7}$$

$$CO \qquad -\frac{\rho D_{CO}}{M_{CO}}\left.\frac{d\omega_{CO}}{dr}\right|_s + \frac{q\omega_{CO}}{M_{CO} r_s} = 2\left(R_{O_2} + R_{CO_2}\right) \tag{8}$$

$$\tau \qquad -\lambda T_b \frac{d\tau}{dr} = H_{O_2} R_{O_2} - H_{CO_2} R_{CO_2} \tag{9}$$

The boundary conditions at the edge of the stagnant film are:

$$\omega_{O_2} = \omega_{O_{2B}} \tag{10}$$

$$\omega_{CO_2} = \omega_{CO_{2B}} = 1 - \omega_{O_{2B}} \tag{11}$$

$$\omega_{CO} = 0 \tag{12}$$

$$\tau = 1 \tag{13}$$

Equations (2) and (3), (4) and (3), and (5) and (3) were combined to eliminate R_{CO}. The equations were solved yielding

$$\omega_{O_2} = -\frac{M_{O_2}}{2M_c} + \left(\omega_{O_{2B}} + \frac{M_{O_2}}{2M_{CO_2}}\omega_{O_{2B}} + \frac{M_{O_2}}{2M_c}\right)\left(\frac{r}{r_b}\right)^{\gamma} - \frac{M_{O_2}}{2M_{CO_2}}\omega_{CO_2} \tag{14}$$

$$\omega_{CO} = \frac{M_{CO}}{M_c} + \left(\frac{M_{CO}}{M_{CO_2}}\omega_{CO_{2B}} - \frac{M_{CO}}{M_c}\right)\left(\frac{r}{r_b}\right)^{\gamma} - \frac{M_{CO}}{M_{CO_2}}\omega_{CO_2} \tag{15}$$

$$-2\beta\tau + \omega_{CO_2} = \left[2\beta(\tau_s - 1) + \xi + \omega_{O_{2B}}\right]\left(\frac{r}{r_b}\right)^{\gamma} - 2\beta\tau_s - \xi \tag{16}$$

where

$$\gamma = \frac{q}{\rho D} \qquad \beta = \frac{M_{CO_2} C_p T_b}{W_{CO}} \qquad \xi = \frac{M_{CO_2} H_{O_2}}{M_c W_{CO}}$$

These equations were used to find the range of γ that would allow a feasible solution. Feasible solutions are those where ω_{CO_2}, ω_{O_2}, and ω_{CO} have values equal to or greater than zero but less than or equal to one. The surface temperature was picked and the equations were solved for ω_{CO_2}, ω_{O_2}, and ω_{CO} varying the value of γ. The gas phase reaction between CO and O_2 was assumed to be first order with respect to both CO and O_2.

$$R_{CO} = KC_{CO}C_{O_2} \exp\left(-\frac{E}{RT}\right) \tag{17}$$

This equation was substituted into equation (4) and (14) to (16) were rearranged so that ω_{O_2} and τ were functions of ω_{CO}. These expressions were then substituted into equation (17), and the resulting equation was solved using a Runge-Kutta technique. The physical properties used in the equation are available in reference 1. The surface reaction rates used were taken from reference 11. Also, reference 11 presents the conclusions of Valis who determined that the activation energy for the reaction of carbon dioxide and carbon is 2.2 times the activation energy for the reaction of oxygen with carbon, and the pre-exponential factor can be obtained from the equation

$$K = K_o \exp\left[\frac{E}{R}\left(\frac{1}{T^*} - \frac{1}{T_s}\right)\right] \tag{18}$$

where

K_o = 31.6 cm/sec, T* = 1240 K for reaction of carbon and oxygen

T* = 1840 K for reaction of carbon with carbon dioxide.

The reaction rates given by these relationships were also used. In the solution the pre-exponential factor was the variable with all other parameters being fixed.

The solution of the model equations with parameters that resulted in the best fit with the experimental data are presented in figures 26 and 27. In both figures the parameters for the model are the same. The differences between the model and experimental data are attributed to free convective effects. Figure 26 compares the model with the concentration profiles obtained with the sample probe at the 90° position. The trend of the O_2 profiles are similar, but the experimental data are approximately 0.1 mole fraction higher than the model. There is a significant difference between the experimental and calculated profiles for CO_2 between the surface and

0.165 cm from the surface. At distances from the surface greater than 0.165 cm, the experimental and calculated profiles have the same trend, but the experimental profile is 0.07 mole fraction lower than the calculated profile. The experimental and calculated CO profiles have the same trend at distances from the surface greater than 0.165 cm, with the experimental profile being 0.04 mole fraction lower than the calculated profile. At 0.165 cm from the surface, the two profiles diverge as the distance from the surface decreases.

The experimental concentration profiles obtained with the sampling probe at the 45° position are compared with the calculated profiles in figure 27. The experimental and calculated O_2 profiles are closer for this case but the experimental profile increases more rapidly than the calculated profile and they eventually cross at 0.053 cm from the surface. Also, near the surface the slope of the calculated profile is at its lowest, while the slope of the experimental profile is at its highest. The maximum difference between the two profiles is less than 0.1 mole fraction. Again there is a significant difference for the CO_2 profiles between the surface and 0.165 cm away from the surface. The slopes of the two profiles near the surface are different, with the experimental profile slope being negative while the calculated profile slope is positive. The CO profiles have the same trend at distances greater than 0.165 cm from the surface, with the experimental profile being 0.02 mole fraction lower than the calculated profile. As the distance to the surface is decreased from 0.165 cm, the profiles diverge.

CONCLUSIONS FOR NORMAL GRAVITY

For a carbon rod burning in a dry oxygen environment, there is a gas phase reaction in which CO is burned to CO_2. From a 90° position to the top of the rod, the O_2 concentration decreases, the CO_2 concentration increases except near the surface where it is the lowest at the top of the rod, and the CO in general increases. This means that convective effects are playing a considerable role in the combustion process, decreasing the oxygen supply to the rod by convecting up the combustion products. This convective mass transfer process is considerably faster than the radial gas diffusion process, as is evidenced by the disagreement between the model and the experimental data. The surface reaction at 90° and 45° from the top of the rod is controlled by chemical kinetics, while the reaction at the top of the rod may be controlled by diffusion.

GENERAL CONCLUSIONS

To learn more about the role of convection as it affects the mechanism of oxidation in this combustion process, a long term zero gravity experiment is needed. This would eliminate the strong normal gravity convective effects and allow for long term gas sampling and temperature measurements. The surface temperature, concentration profiles, and temperature profiles, that would be obtained, are needed to completely describe the zero-gravity carbon combustion process.

NOMENCLATURE

C	concentration
C_p	specific heat
D	diffusion coefficient
E	activation energy
H	heat of combustion
K	pre-exponential factor
M	molecular weight
R	reaction rate
$\bar{R}$	universal gas constant
$\dot{R}$	reaction rate
r	radius
T	temperature
V	radial velocity
W_{CO}	heat of combustion of two moles of CO
x	mole fraction
λ	thermal conductivity
ρ	density
τ	dimensionless temperature T/T_b
ω	mass fraction

Subscripts:

B	edge of stagnant film
s	surface of rod
CO	carbon monoxide
CO_2	carbon dioxide
O_2	oxygen

REFERENCES

1. Spuckler, C. M., "Combustion of Carbon Rods in Zero and Normal Gravity," PhD thesis, The University of Toledo, Toledo, Ohio (1979).

2. Ubhayakar, S. K., and F. A. Williams, "Burning and Extinction of a Laser Ignited Carbon Particle in Quiesent Mixtures of Oxygen and Nitrogen," J. Electrochem. Soc., 123, 747-756 (May 1976).

3. Fendell, F. E., "The Burning of Spheres Gasified by Chemical Attack," Combust. Sci. Technol., 1, 13-24 (July 1969).

4. Wicke, E. and G. Wurzbacher, "Concentration Profiles in Front of a Carbon Surface Burning in a Flow of Oxygen," NASA TT F 16813 (Dec. 1975).

5. Caram, H. S. and N. R. Amundson, "Diffusion and Reaction in a Stagnant Boundary Layer about a Carbon Particle," Ind. Eng. Chem. Fundam., 16 (2), 171-181 (1977).

6. Spalding, D. B., "Combustion of Fuel Particles," Fuel, 30 (6) 121-130 (June 1951).

7. van der Held, E. F. M., "The Reaction Between a Surface of Solid Carbon and Oxygen," Chem. Eng. Sci., 14, 300-313 (1961).

8. Stearns, C. A., et. al., NASA TM 73720 (1977).

9. Mann, J. B., "Ionization Cross Sections of the Elements," in Recent Developments in Mass Spectrometry, K. Ogata and T. Hayakawa, Eds., pp. 814-819, University Park Press, Baltimore (1971).

10. Brabbs, T. A., et. al., "Shock Tube Measurements of Specific Rates in the Branched Chain H_2-CO-O_2 System," International Symposium on Combustion, 13th, pp. 129-136, The Combustion Institute, Pittsburgh (1971).

11. Frank-Kamenetskii, D. A., Diffusion and Heat Exchange in Chemical Kinetics, Princeton Univ. Press, Princeton, New Jersey (1955).

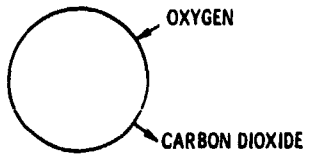

SURFACE REACTION: $C + O_2 \rightarrow CO_2$

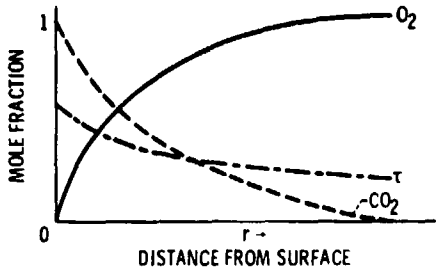

Figure 1. - Low temperature model.

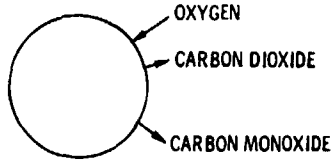

SURFACE REACTIONS: $C + O_2 \rightarrow CO_2$

$2C + O_2 \rightarrow 2CO$

NO GAS PHASE REACTION

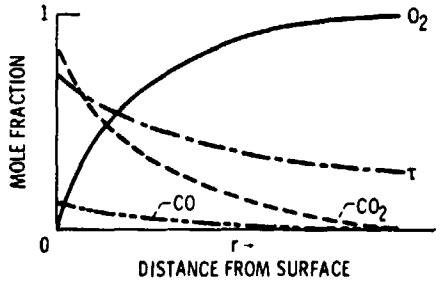

Figure 2. - Mid temperature model.

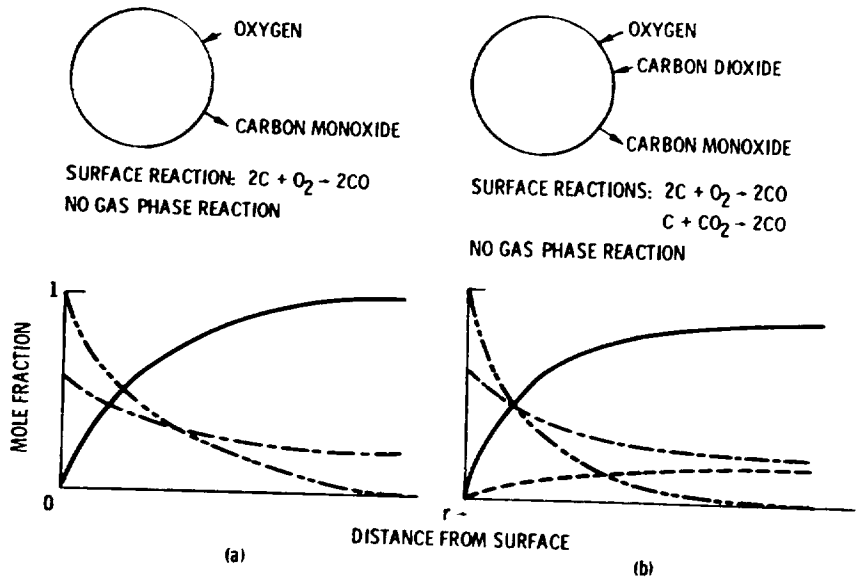

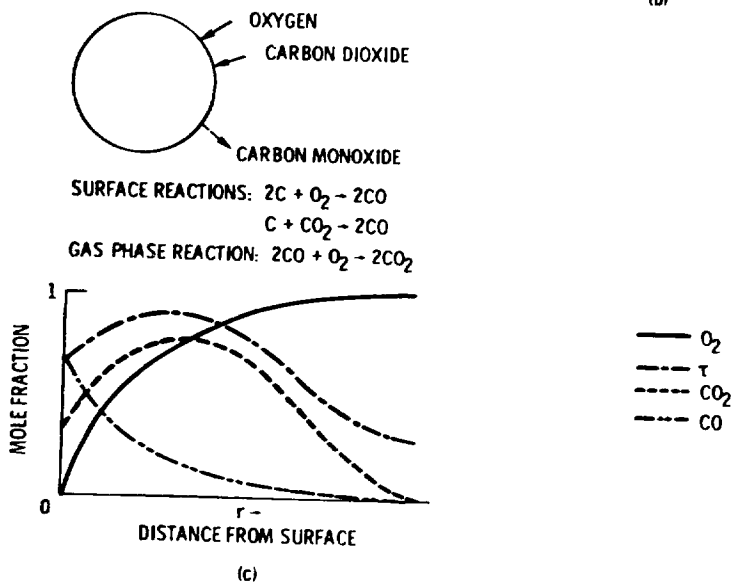

Figure 3. - High temperature model.

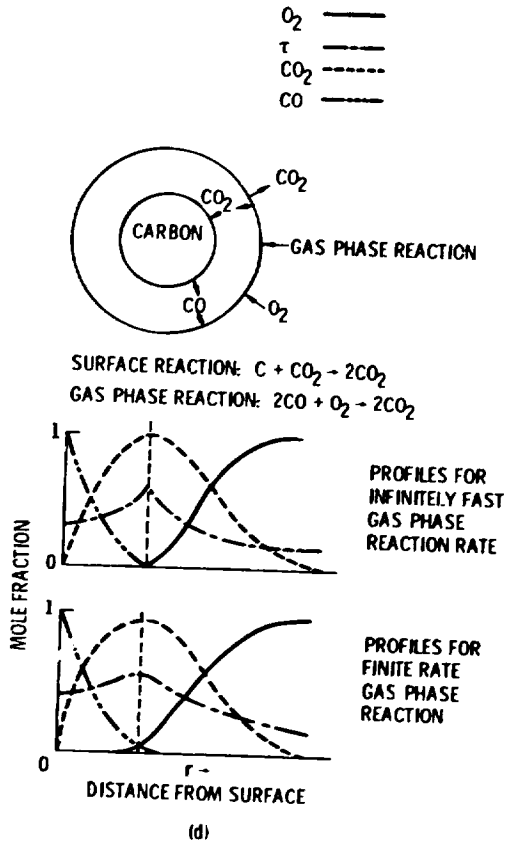

Figure 3. - Concluded.

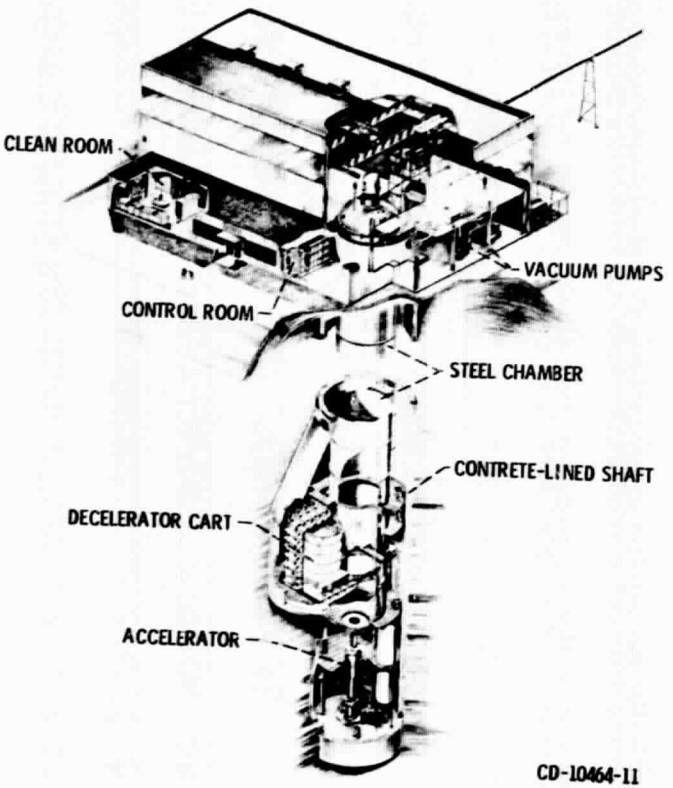

Figure 4. - Schematic diagram of 5- to 10-second zero-gravity facility.

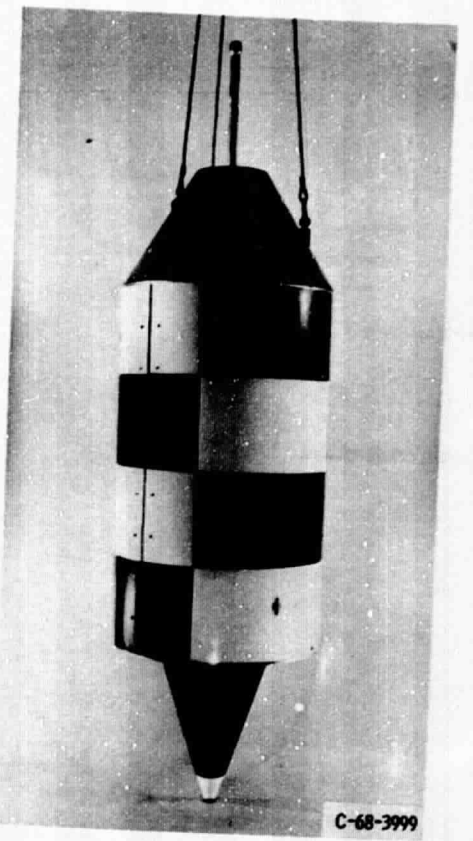

Figure 5. - Experiment vehicle.

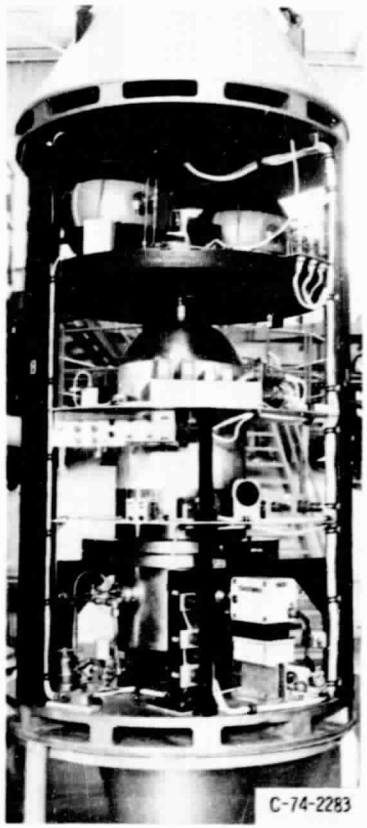

Figure 6. - Test rig.

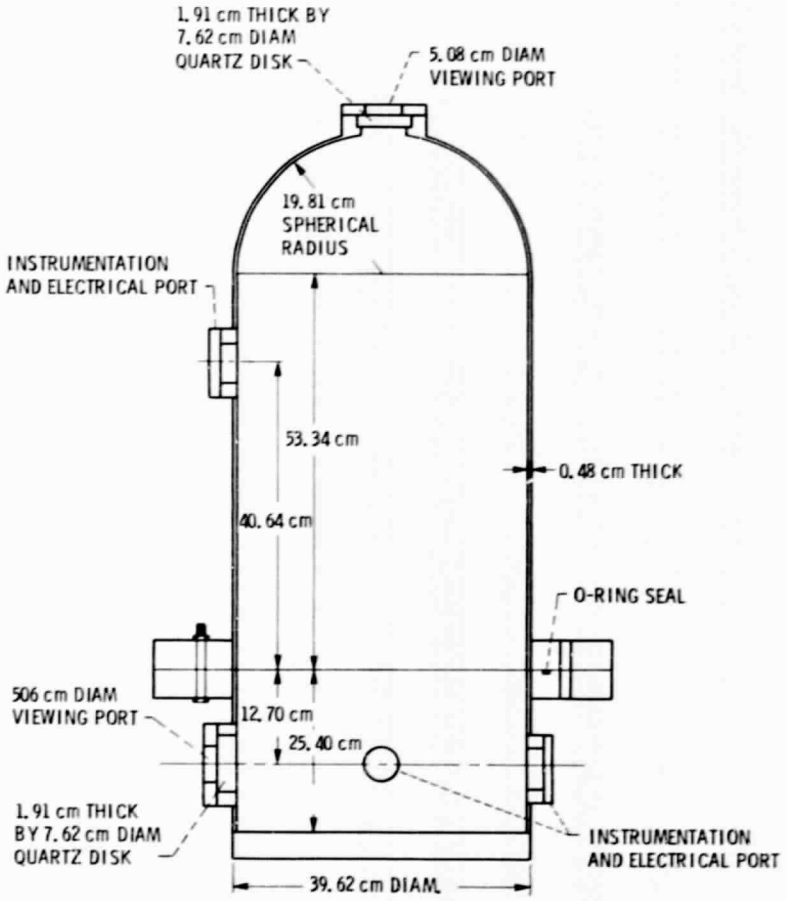

Figure 7. - Cross-sectional schematic of combustion chamber.

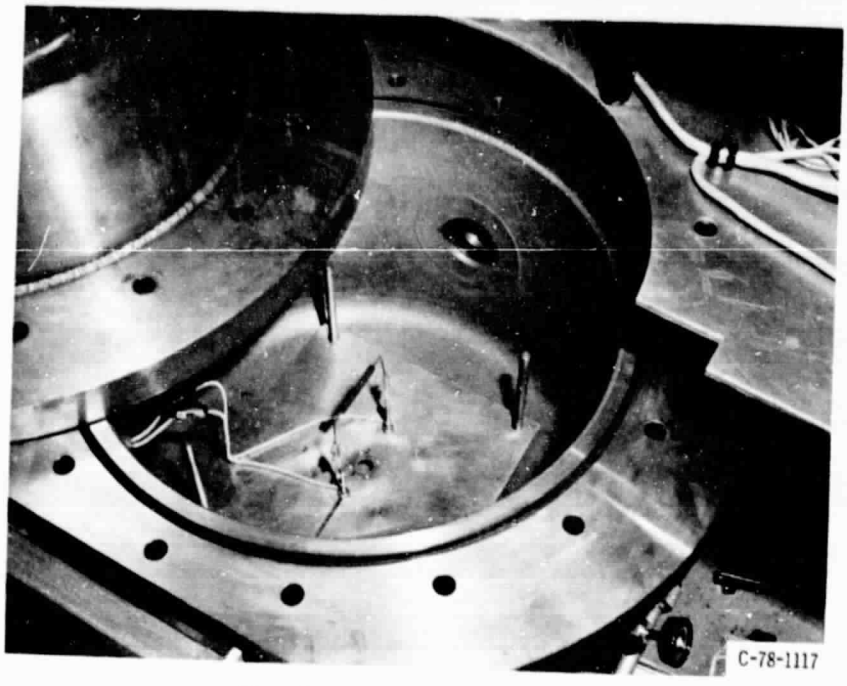

C-78-1117

Figure 8. - Carbon rod in burning chamber.

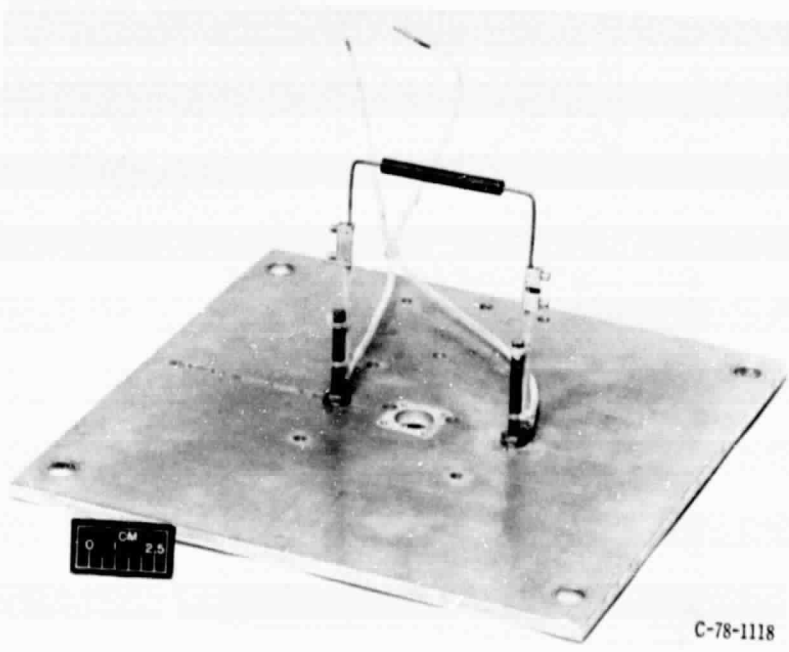

C-78-1118

Figure 9. - Carbon rod holder.

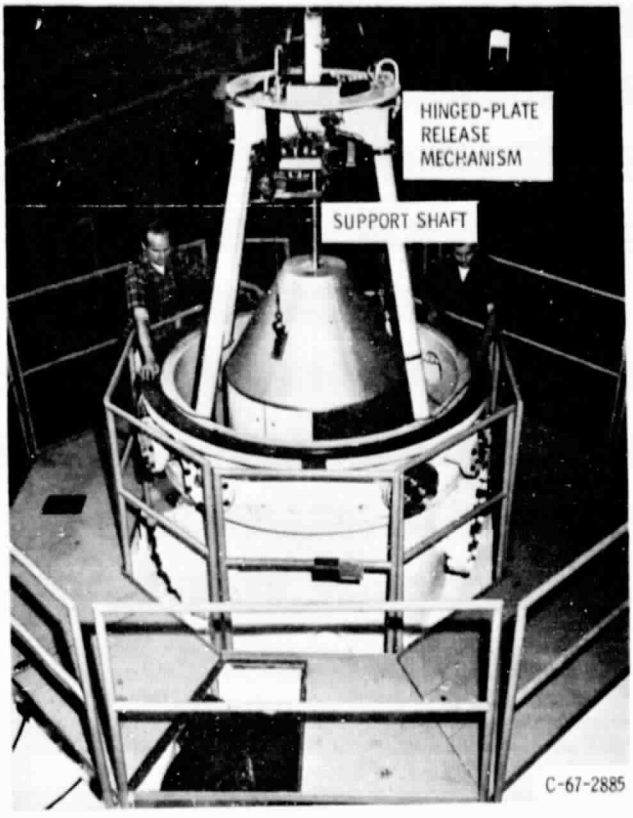

Figure 10. - Typical vehicle positioning prior to release.

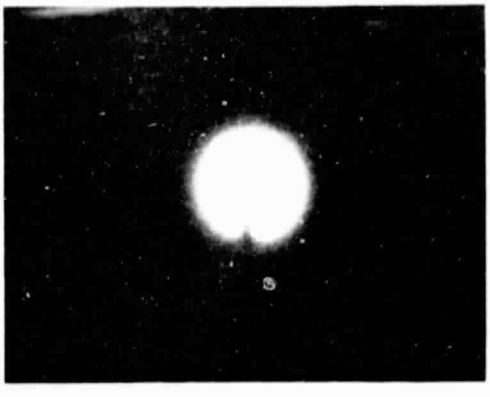

Figure 11. - Carbon rod burning in 1.38×10^5 N/m^2 (20 psia) oxygen environment.

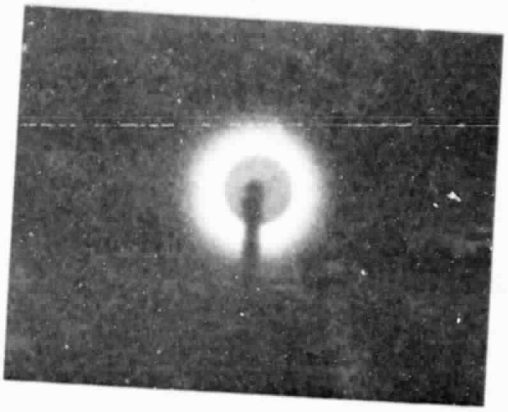

Figure 12. - Carbon rod burning in 3.45×10^4 N/m^2 (5 psia) oxygen environment.

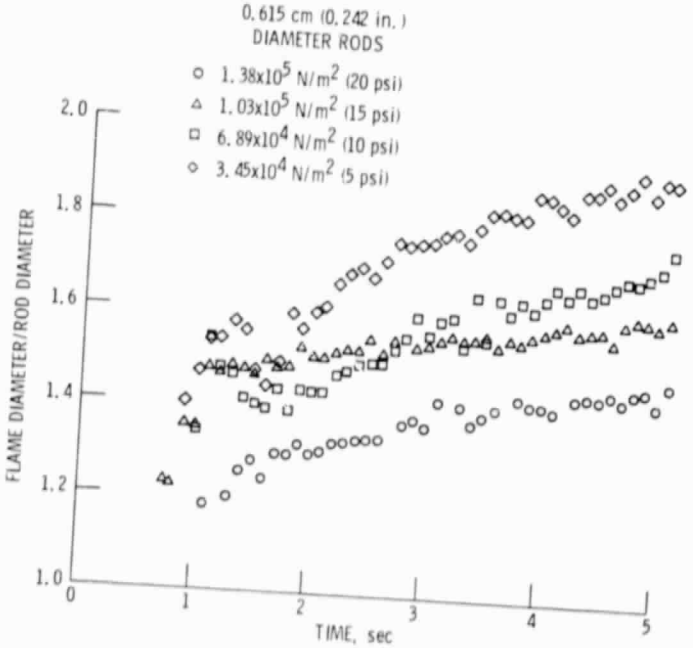

Figure 13. - Flame diameter/rod diameter as a function of time for various pressures.

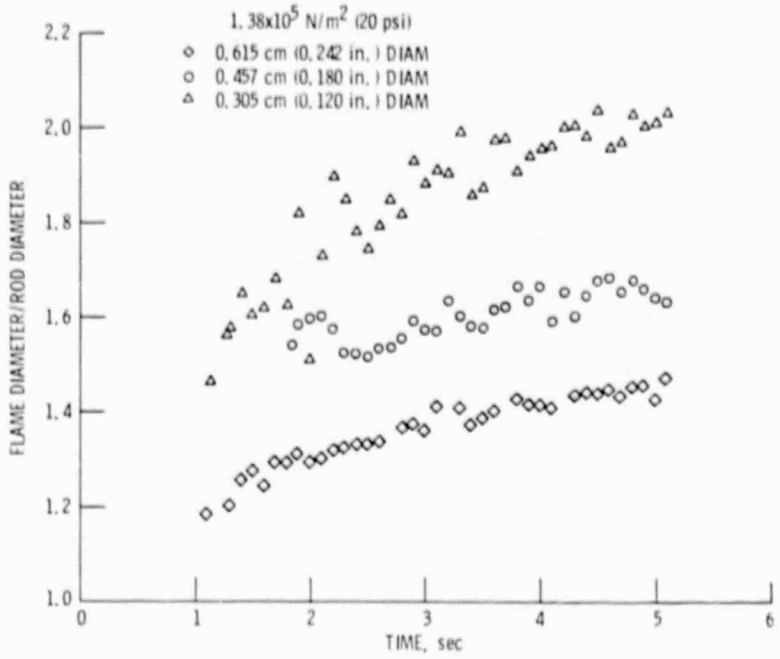

Figure 14. - Flame diameter/rod diameter as a function of time for various diameter rods.

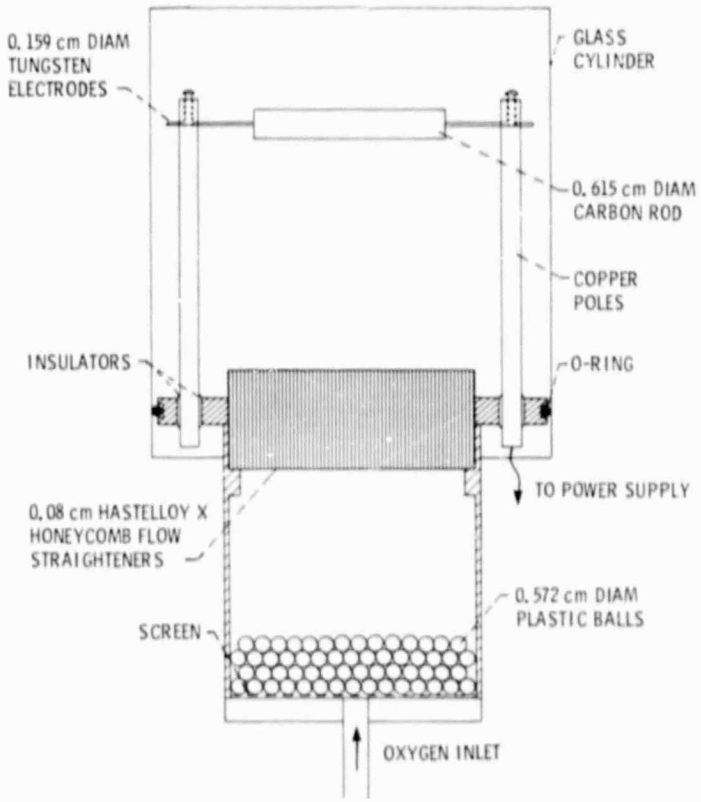

Figure 15. - Schematic of carbon rod burning apparatus.

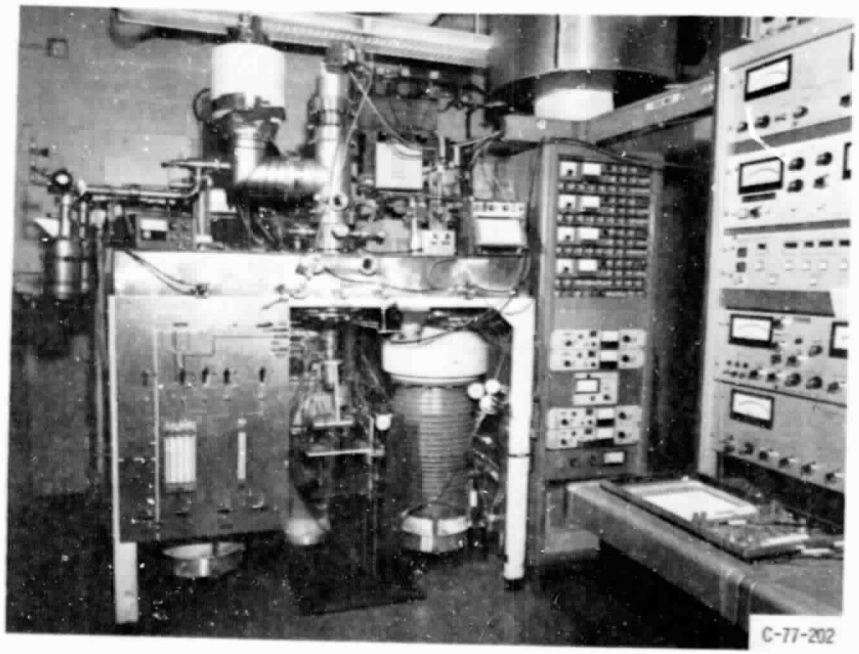

Figure 16. - Mass spectrometric sampler.

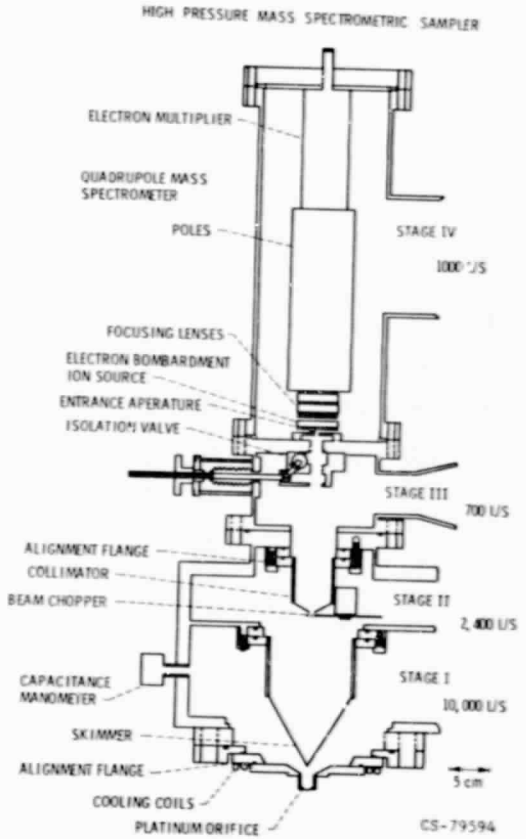

Figure 17. - Schematic of spectrometric sampler.

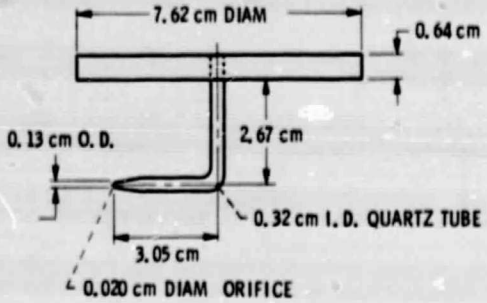

Figure 18. - QUARTZ gas sampling probe.

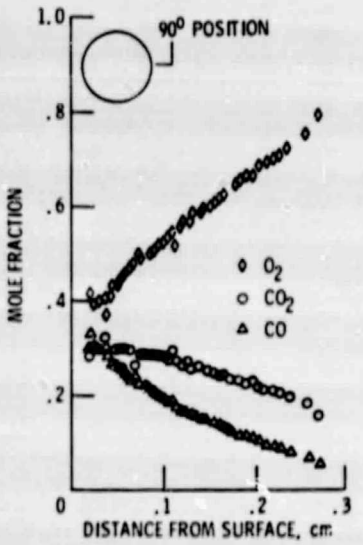

Figure 19. - Concentration as a function of distance from surface-probe at 90°.

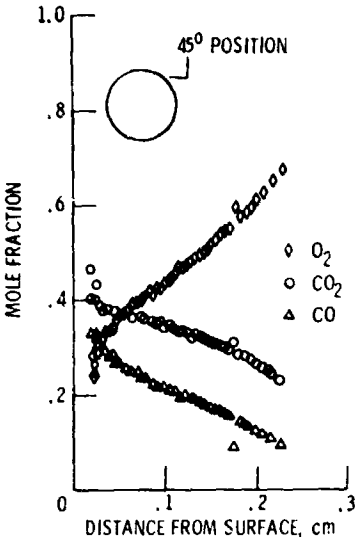

Figure 20. - Concentration as a function of distance from surface-probe at 45°.

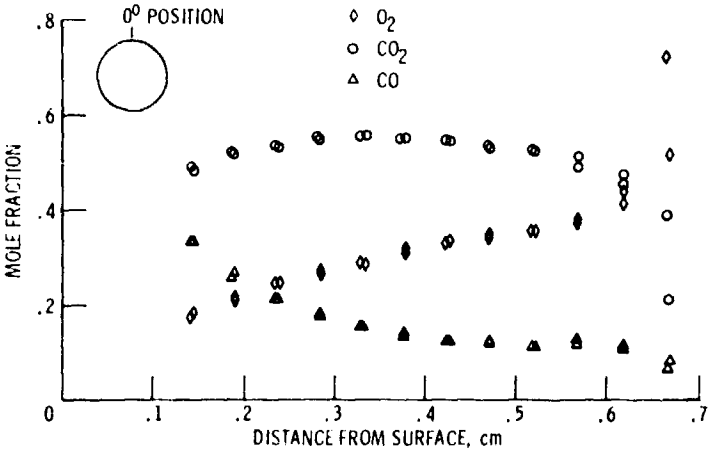

Figure 21. - Concentration as a function of distance from surface probe at 0°.

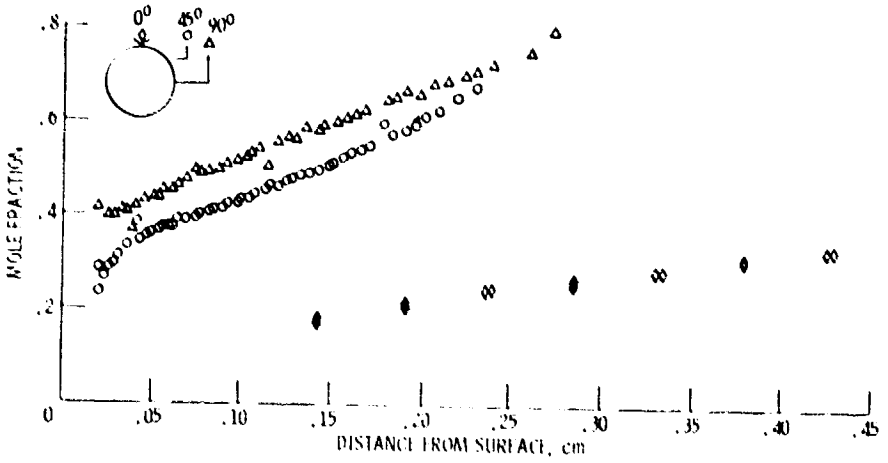

Figure 22. O_2 concentration as a function of distance from surface for various gas sampling probe positions.

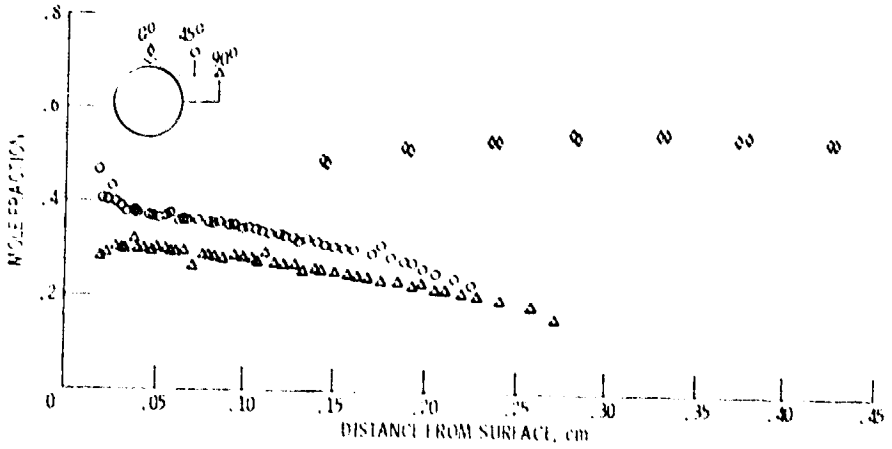

Figure 23. CO_2 concentration as a function of distance from surface for various gas sampling probe positions.

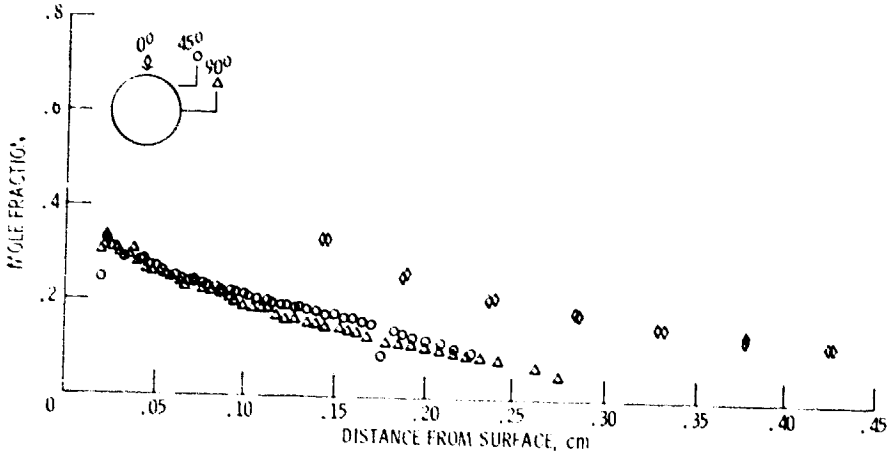

Figure 24. - CO concentration as a function of distance from surface for various gas sampling probe positions.

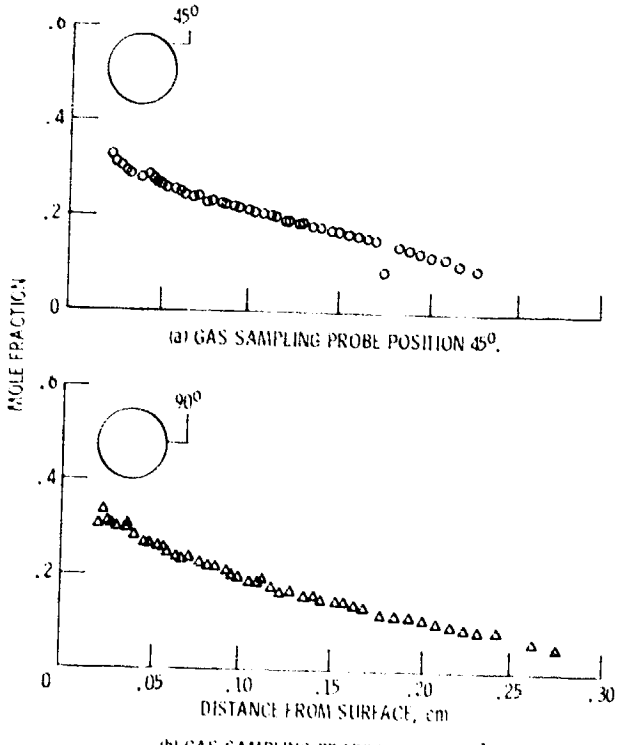

(a) GAS SAMPLING PROBE POSITION 45°.

(b) GAS SAMPLING PROBE POSITION 90°.

Figure 25. - CO concentration as a function of distance from surface.

$R_{O_2} = 4.132 \times 10^{-6}$ g mole/cm^2 sec

$R_{CO_2} = 7.607 \times 10^{-4}$ g mole/cm^2 sec

E = 4100 cal/g mole (REF. 10)

K = 2.763×10^{10} cm^3/g mole sec

$X_{O_{2S}} = 0.327$ $X_{O_{2B}} = 0.925$

$X_{CO_{2S}} = 0.041$ $X_{CO_{2B}} = 0.075$

$X_{CO_S} = 0.623$ $T_S = 1542$ K

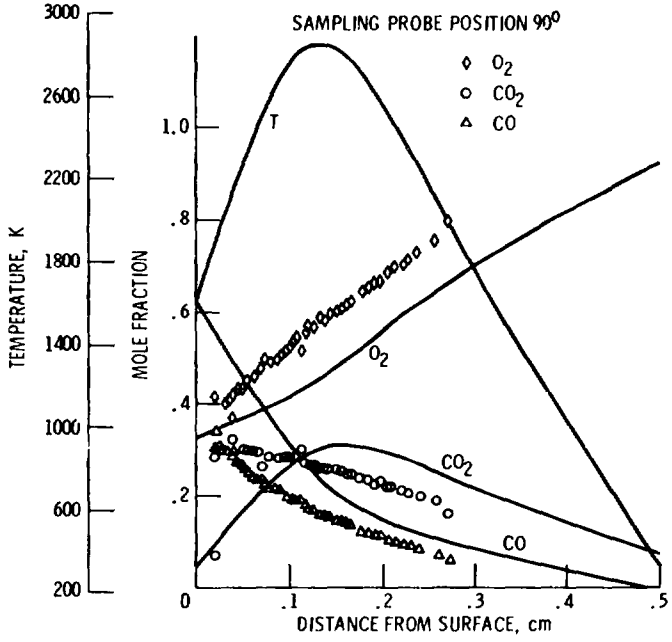

Figure 26. - Comparison of model with experimental data - probe position 90°.

$R_{O_2} = 4.132 \times 10^{-6}$ g mole/cm^2 sec

$R_{CO_2} = 7.607 \times 10^{-4}$ g mole/cm^2 sec

E = 4100 cal/g mole (REF. 10)

K = 2.763×10^{10} cm^3/g mole sec

$X_{O_{2S}} = 0.327$ $X_{O_{2B}} = 0.925$

$X_{CO_{2S}} = 0.041$ $X_{CO_{2B}} = 0.075$

$X_{CO_S} = 0.623$ $T_S = 1542$ K

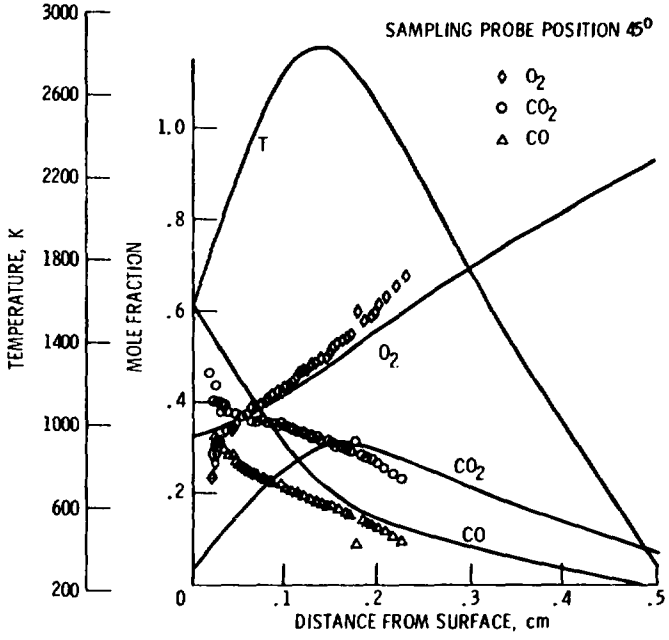

Figure 27. - Comparison of model with experimental data - probe position 45°.